Environ. Sci. Technol. **2010,** *44,* 1698–1704

Response of a Macrotidal Estuary to Changes in Anthropogenic Mercury Loading between 1850 and 2000

ELSIE M. SUNDERLAND,*,† JOHN DALZIEL,‡ ANDREW HEYES,§ BRIAN A. BRANFIREUN,|| DAVID P. KRABBENHOFT,⊥ AND FRANK A.P.C. GOBAS#

School of Engineering and Applied Sciences, Harvard University, Cambridge Massachusetts 02138, Meteorological Service of Canada, Environment Canada, 45 Alderney Drive, Dartmouth, Nova Scotia, B2Y 2N6, Canada, Chesapeake Biological Laboratory, University of Maryland Center for Environmental Science, University System of Maryland, Solomons, Maryland 20688, Department of Geography, University of Toronto at Mississauga, 3359 Mississauga Road North, Mississauga, Ontario, L5L 1C6, Canada, U.S. Geological Survey, 8505 Research Way, Middleton, Wisconsin 53562, and School of Resource and Environmental Management, Simon Fraser University, Burnaby, British Columbia, V5A 1S6, Canada

Received October 26, 2009. Revised manuscript received January 10, 2010. Accepted January 18, 2010.

Methylmercury (MeHg) bioaccumulation in marine food webs poses risks to fish-consuming populations and wildlife. Here we develop and test an estuarine mercury cycling model for a coastal embayment of the Bay of Fundy, Canada. Mass budget calculations reveal that MeHg fluxes into sediments from settling solids exceed losses from sediment-to-water diffusion and resuspension. Although measured methylation rates in benthic sediments are high, rapid demethylation results in negligible net in situ production of MeHg. These results suggest that inflowing fluvial and tidal waters, rather than coastal sediments, are the dominant MeHg sources for pelagic marine food webs in this region. Model simulations show water column MeHg concentrations peaked in the 1960s and declined by almost 40% by the year 2000. Water column MeHg concentrations respond rapidly to changes in mercury inputs, reaching 95% of steady state in approximately 2 months. Thus, MeHg concentrations in pelagic organisms can be expected to respond rapidly to mercury loading reductions achieved through regulatory controls. In contrast, MeHg concentrations in sediments have steadily increased since the onset of industrialization despite recent decreases in total mercury loading. Benthic food web MeHg concentrations are likely to continue to increase over the next several decades at present-day mercury emissions levels because the deep active sediment layer in this system contains a large amount of legacy mercury and requires hundreds of years to reach steady state with inputs.

* Corresponding author e-mail: ems@seas.harvard.edu.
† Harvard University.
‡ Environment Canada.
§ University of Maryland Center for Environmental Science.
|| University of Toronto at Mississauga.
⊥ U.S. Geological Survey.
Simon Fraser University.

Introduction

High levels of exposure to methylmercury (MeHg) from fish consumption causes adverse health effects on humans and wildlife (*1, 2*). Approximately 90% of fish consumed in the U.S. population are from estuarine and marine systems (*3*). Since MeHg is actively produced in coastal and shelf sediments (*4*−*6*) and tidal salt marshes (*7*), these systems are an important vector for entry of MeHg into marine food webs. Evaluating the magnitude of Hg loading reductions needed to maintain fish tissue levels below regulatory guidelines considered safe for human consumption requires a quantitative analysis of estuarine mercury (Hg) cycling processes (*8*). Here we develop an ecosystem model of Hg dynamics to investigate anthropogenic impacts on estuarine MeHg levels. To do this, we reconstruct historical mercury loading (1850−2000) from atmospheric deposition, tides, and rivers to a coastal embayment in eastern Canada using sediment core data and global models.

Anthropogenic Hg emissions in eastern Canada and the northeastern United States peaked in the 1970s and have declined by over 50% since this time (*9, 10*). Despite these reductions in emissions, Hg concentrations in some freshwater and marine fish and wildlife remain high (*11, 12*). Fish consumption advisories throughout this region warn of health risks associated with Hg exposure for pregnant women and other sensitive groups (*13*). Time scales required for Hg to cycle through freshwater and marine ecosystems are highly variable and can range from several years to many decades (*14*−*17*). Environmental fate and bioaccumulation models are critical for synthesizing best-available process understanding and for determining how the legacy of anthropogenic Hg loading has affected biological MeHg concentrations. Such information is essential for developing effective management strategies and emission reduction targets. Here we develop such a fate and transport model and apply it to Passamaquoddy Bay, a macrotidal estuary located at the mouth of the Bay of Fundy, Canada. This region has historically supported large fish populations and provides critical habitat for wildlife (*18*), in part due to its unique hydrography and extreme tidal range that reaches up to 16 m at the mouth of the Bay of Fundy (*19*). Protecting coastal water quality is vital for the local economy because approximately 20,000 U.S. and Canadian fishers depend on marine resources in this region (*20*).

This study's main objective is to develop an analytical framework for better understanding the biogeochemical cycling of Hg in coastal ecosystems. The model developed here simulates changes in MeHg concentrations between 1850 and 2000 using the trajectory of historical loading from several data sources (*4, 16, 21*). We evaluate the model's performance using sensitivity analyses and by comparing results to measurement data from our previous research (*4, 21*−*24*). We apply the model to (a) quantify the relative importance of different sources of mercury loading (atmospheric, tidal, riverine); (b) characterize time scales required for anthropogenic Hg to cycle through this ecosystem; and (c) assess impacts of anthropogenic Hg on MeHg reservoirs and fluxes driving the bioavailable Hg pool at the base of the food web. To our knowledge, this is the first ecosystem-scale simulation of how changing loading from anthropogenic sources over the last 150 years has impacted estuarine MeHg levels.

Methods

Site Description. Passamaquoddy Bay is a semienclosed macrotidal estuary (Figure 1). Strong currents and tidal mixing

10.1021/es9032524

Published on Web 02/01/2010

inhibit thermal stratification of the water column during summer months. Forests cover most of the watershed (4225 km^2), with the exception of a narrow floodplain that supports mixed farming and light industry (*25*). Water temperatures vary from a low of −1 C in winter to 16 C in summer (*26*). The average water depth is 30 m (maximum of ∼70 m) and salinities range between 26‰ and 33‰ (*26*). As a smaller and tidally dynamic system enclosed by the Bay of Fundy, Passamaquoddy Bay differs from previously studied larger estuaries such as Long Island Sound (*27*) and Chesapeake Bay (*28*) that have much longer water residence times.

General Model Description. We developed equations to describe the transport and partitioning of each of the three main forms of mercury (elemental Hg: Hg(0), divalent Hg: Hg(II), and MeHg) in water and sediments (Supporting Information (SI) Figure S1) using the general fate and transport modeling framework developed by Gobas et al. (*29, 30*). All model compartments are assumed to be well-mixed, and benthic sediments are divided into an active layer and a truly buried inaccessible sediment layer (*4*). External loading from atmospheric deposition (*A*), rivers (*R*), and tidal inflow (TL) drives the model, which is run with a temporal resolution (*t*) of one day. A larger time-step results in numerical instability because many of the reaction rates are very fast (e.g., oxidation and reduction). One-step forward Euler-type numerical integration is used to compute changes in the mass of each Hg species in water (M_w) and sediments (M_s) over time. For total Hg this is represented by the following general equations:

$$\frac{dM_w}{dt} = (A + R + \mathrm{TL}) + (k_{res} + k_{diff})M_s - (k_{ev} + k_o + k_{sett})M_w \quad (1)$$

$$\frac{dM_s}{dt} = k_{sett}M_w - (k_{res} + k_{bur} + k_{diff})M_s \quad (2)$$

Rate coefficients (d^{-1}) shown in eqs 1 and 2 and Figure S1 represent tidal outflow (k_o), sediment resuspension (k_{res}), sediment settling (k_{sett}), diffusion (k_{diff}), burial (k_{bur}), and Hg(0) evasion (k_{ev}). Rates of interspecies conversions in the differential equations for MeHg, Hg(0) and Hg(II) (SI Section II, Figure S1) are described using rate coefficients for Hg(II) reduction (k_{red}), Hg(0) oxidation (k_{ox}), Hg(II) methylation (k_m), MeHg demethylation (k_{dm}), and MeHg photodecomposition (k_{dmw}). All rate coefficients represent annually averaged values and include in their calculation partitioning of Hg species between the dissolved and solid phases (see SI for details). Additional information on methods and data used to derive model rate coefficients is provided in SI Section IV.

External Inputs from Rivers, Tides, and Atmospheric Deposition. In previous research, we estimated mean anthropogenic enrichment factors (AEF = 2000 loading/1850 loading) for atmospheric deposition (3.2 ± 0.4) and freshwater inputs (3.6 ± 1.9). Here we reconstruct annual loading between 1850 and 2000 by combining measured present-day (year 2000) inputs with historical loading information from sediment cores and global models. For atmospheric deposition and fluvial inputs, we multiplied measured contemporary inputs by the relative changes in loading indicated by sediment core data (*4, 21*). Sediment cores used to reconstruct historical atmospheric deposition were from

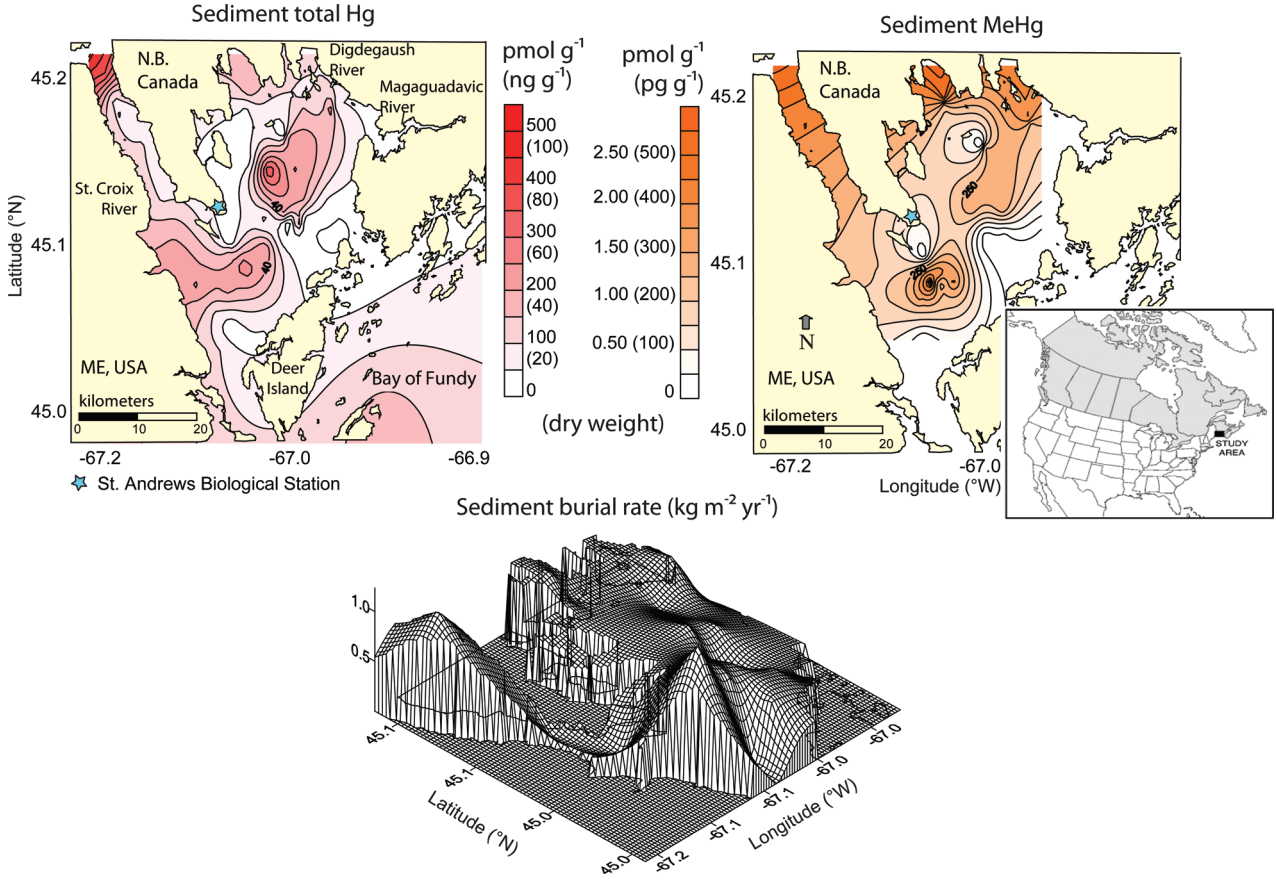

FIGURE 1. Map of study region showing spatially interpolated measured total Hg and MeHg concentrations and burial rates used to calculate the contemporary (ca. 2000) reservoirs in sediments and burial fluxes. Information on sampling locations, analytical methods, and correlations with ancillary sediment characteristics can be found in Sunderland et al. (*4, 24*).

tidal salt marshes, lakes, and bogs in the region, while cores from the mouth of the St. Croix River (the major freshwater tributary) were used to reconstruct historical loading from rivers. To characterize changes in Hg fluxes from tidal inflows, we used data from Sunderland and Mason (*16*) showing the Atlantic Ocean (35 S−55 N) has been enriched in total Hg by 58% since preindustrial times. Because no historical oceanic Hg trend data are available, we assume that changes in tidal inputs increase linearly between 1850 and 2000 to the contemporary enrichment level (*16*).

Year 2000 inputs are based on measured Hg concentrations and hydrological fluxes for each source. Inflowing tidal water volume (T_i) is estimated from the difference between tidal outflow (T_o) and the sum of freshwater inflow (R) and inputs through precipitation (P) (i.e., $T_i = T_o - R - P$). Concentrations of Hg species in tidal water are based on data from Dalziel et al. (*22*), who measured unfiltered seawater concentration profiles at 15−50 m vertical intervals in the Bay of Fundy between 2000 and 2002 (mean Hg: 1.20 ± 0.34 pM; mean MeHg: 0.29 ± 0.11 pM). No data are available for Hg(0), therefore we assumed that the fraction of total Hg present as Hg(0) in tidal waters is 13 ± 6% corresponding to the overall mean and standard deviation of the fraction present in the Atlantic Ocean at comparable latitudes compiled by Sunderland and Mason (*16*).

Monthly fluvial discharges into Passamaquoddy Bay are reported by Gregory et al. (*19*). Annually averaged Hg concentrations in the three major freshwater tributaries (Hg: 19.0 ± 7.6 pM; MeHg: 1.22 ± 0.25 pM) are based on previous studies (*22, 31*) that measured unfiltered Hg concentrations and suspended particulate content over several seasons (SI Table S2). Total (wet + dry) atmospheric deposition (54.8 ± 0.5 nmol m^{-2} yr^{-1}) is based on measurements and models described in detail elsewhere (*21*). Wet atmospheric deposition rates (mean 30.9 ± 6.7 nmol m^{-2} yr^{-1}) were taken from measurements at the St. Andrews Mercury Deposition Network (MDN) Station (NB-02) (SI Table S2). Inputs of MeHg in precipitation are from Environment Canada measurements at nearby field stations showing MeHg is on average 1.6 ± 1.2% of total Hg in precipitation (*22*).

Empirically Constrained Mass Budget. We developed an empirically constrained mass budget for the year 2000 using measured sediment and water concentrations. We used depth integrated seawater concentrations for total Hg (1.27 ± 0.23 pM) and MeHg (0.25 ± 0.07 pM) measured in Passamaquoddy Bay (November 2001) and the four closest Bay of Fundy sampling stations (June 2001−August 2002) (SI Table S2) to characterize the contemporary water column reservoirs of total Hg and MeHg (*22*). Because no direct measurements of Hg(0) concentrations in seawater are available, we specified rate coefficients for oxidation and reduction measured in other coastal systems (SI Section IV) and allowed concentrations to reach steady state. We also estimated the accumulation of Hg and MeHg in primary producers based on a reported primary productivity of 296 g C m^{-2} yr^{-1} (*32*), measured concentrations in dinoflagellates and diatoms (total Hg: 14.0 ± 4.1 and MeHg: 0.75 ± 0.55 pmol g^{-1} wet weight) in the Bay of Fundy (*11*), an 80% moisture content, and assumed that 50% of the plankton dry weight is carbon (*32*).

In previous work, we measured a deep active sediment layer of 0.15 m (*4*) that exchanges Hg with the water column and buried sediments through resuspension, diffusion, and burial (*33*). Spatial heterogeneity in sediment Hg concentrations (*34, 35*) can introduce substantial error into box model calculations that are based on mean concentrations from a limited sampling population. To account for this heterogeneity, we spatially interpolated measurement data for total Hg (n = 56) and MeHg (n = 52) reported in our previous work (*4, 24*) using several algorithms (Variogram, Drift Type, and Nugget Effect models) (*36*). Sediment reservoir calculations were completed by summing volume estimates for each cell defined in the spatial grid (see burial flux diagram Figure 1) using the Trapezoidal Rule, Simpson's Rule, and Simpson's 3/8 Rule, where the difference among methods was used to estimate the error among volume calculations (*37*). Figure 1 shows the spatially interpolated concentrations of total Hg and MeHg in benthic sediments used to derive mass budgets shown in Figure 2.

Preindustrial Budget and Time-Dependent Simulation. We developed a preindustrial budget for Hg by assuming local steady state with 1850 loading, and that no changes in present-day sedimentation rates have occurred in the Bay. We drive the preindustrial steady state model with reconstructed historical loading between 1850 and 2000, and force the simulation for an additional 50 years (to 2050) with constant 2000 loading rates to project changes in water and sediment concentrations over time.

Model Evaluation and Sensitivity Analysis. For all simulations and mass budget calculations we show upper and lower bounds for modeled Hg concentration changes based on 95% confidence intervals for measured inputs from rivers, tides, and atmospheric deposition. We conducted detailed sensitivity analysis on model inputs and parameters, including the net methylation rate in benthic sediments, the reduction rate coefficient, the depth of the active sediment layer, alternate formulations of the gas exchange flux (*38, 39*), and upper and lower bounds for diffusion coefficients (*27, 34*). We also compare results from the time-dependent model simulation to available measured Hg concentrations.

Results and Discussion

Model Evaluation. Comparing model simulated water and sediment Hg concentrations to independent data shows reasonable agreement given the error and uncertainty in historical loading (Figure 3). Year 2000 measurements of water column total Hg and MeHg (Figure 3) suggests that model predicted concentrations are biased slightly high relative to observations. However, natural stochasticity in Hg concentrations (*16*) and limited sample sizes means observations are also subject to error and uncertainty. We could not comprehensively test model performance by comparing results to measurement data because limited information on temporal trends in Hg concentrations are available. We use model sensitivity analysis to further investigate factors controlling results presented in the remaining sections.

MeHg Production and Diffusion from Benthic Sediments. In previous work we measured substantial Hg(II) methylation in sediments (153 pmol m^{-2} d^{-1}). Year 2000 mass budget results shown in Figure 2 indicate that in situ MeHg production in sediments is not the major MeHg source for the water column and pelagic organisms, assuming MeHg from different sources is equally bioavailable. Figure 2 further shows that the sum of MeHg inputs from settling particles and losses from sediment-to-water diffusion and resuspension results in a net contribution from the water column to benthic sediments of at least 25 pmol m^{-2} d^{-1}. Thus, sediments in this system are an overall sink for water column MeHg. Even combining the upper bound for diffusive fluxes of MeHg with the lower bound for Hg(II) (maximizing methylation and minimizing demethylation) does not result in appreciable net MeHg formation in the sediments given the magnitude of inputs from settling particles (Figure 2) and constraints imposed by measured MeHg concentrations in sediments (0.7−0.8% of total Hg in sediments, Figure 1). Time dependent model simulations show MeHg inputs from settling particles are sufficient to account for observed MeHg accumulation in sediments (Figure 3). Even if all MeHg produced in situ were demethylated, it is plausible that MeHg could continue to accumulate in sediments due to

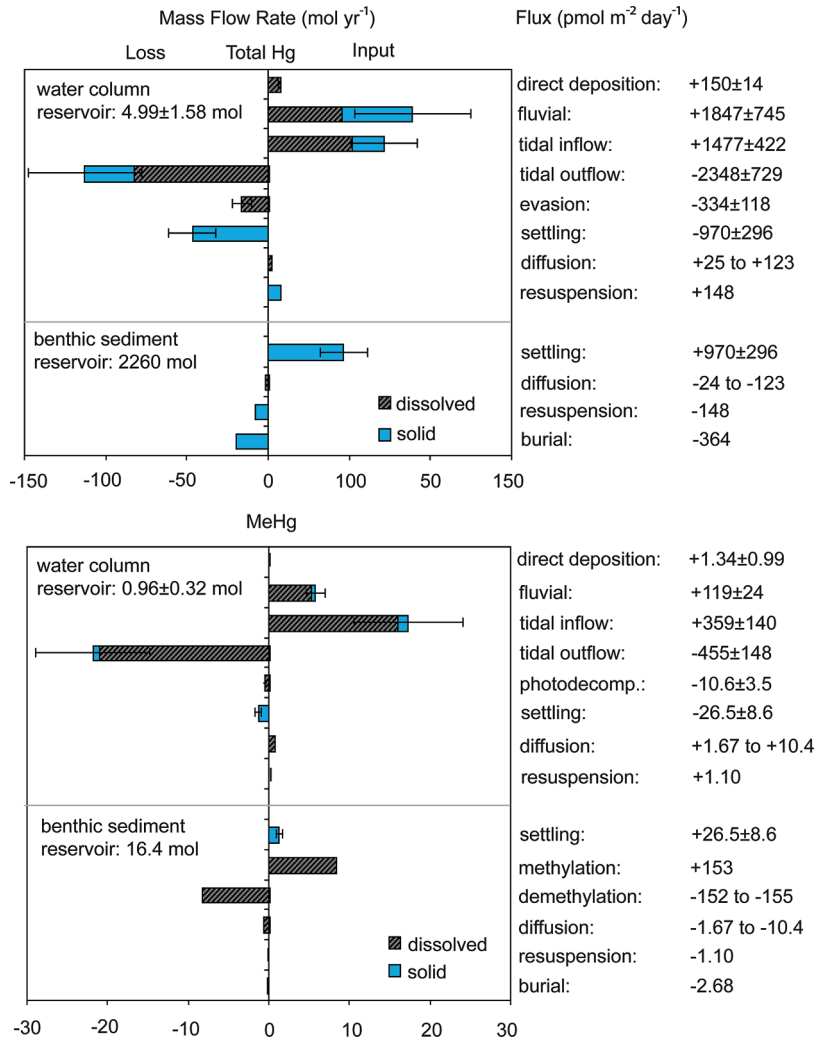

FIGURE 2. Empirically constrained mass budgets for total Hg and MeHg in the year 2000 based on measured water and sediment Hg and MeHg concentrations. Error bars represent 95% confidence intervals around loading and measured concentrations except for sediment reservoirs and mass flow rates, which are based on spatial interpolations of field data. Ranges for diffusion and methylation/demethylation represent scenarios based on high/low diffusion coefficients for Hg species in interstitial waters. Large mass flow rates in the water column compared to the reservoir size results in rapid concentration changes with alterations in inputs, while the larger Hg and MeHg reservoirs and smaller mass flow rates in sediments results in a slower temporal response.

inputs from settling particles, assuming MeHg sorbed to settling solids is sufficiently recalcitrant to survive transit.

Previous studies have constructed estuarine Hg mass budgets without considering the relative magnitude of MeHg inputs to sediments from settling solids (*27, 28, 40*). These studies have postulated that diffusive fluxes of MeHg from estuarine sediments account for the majority of water column MeHg and accumulation in estuarine biota. In contrast, Figure 2 shows that MeHg concentrations in the water column of Passamaquoddy Bay are most affected by external MeHg inputs from tides and rivers (23.1 mol yr^{-1}) rather than MeHg from estuarine sediments (−0.83 mol yr^{-1}). Model sensitivity analysis reveals that increasing the benthic sediment methylation rate by 60% increases water column MeHg concentrations by only 2.1% (SI Figure S2). The relative importance of sediment-to-water diffusion of MeHg compared to external MeHg inputs to the water column (*40*) and/or water column methylation (*41*) could be similarly tested using data from other systems such as Chesapeake Bay and Long Island Sound (*28, 40*).

Although model calculations show that methylation and demethylation rates in sediments are approximately balanced, these processes turn over approximately 50% of the sediment MeHg reservoir on an annual basis (Figure 2). Time-dependent simulations presented in Figure 3 do not account for environmental changes that could alter sedimentary methylation and demethylation rates (*4, 24*). Model sensitivity analysis (SI Figure S2) shows that such changes in the balance of sediment methylation and demethylation would cause large and near proportional changes in sediment MeHg concentrations. Increases in sediment methylation rates could therefore rapidly increase benthic food web exposures.

Water Column Hg Fluxes. For the year 2000 mass budget, the largest inputs of total Hg are from rivers, and the largest output is associated with tidal outflow (Figure 2). Evasion of Hg(0) at the air−sea interface (334 ± 118 pmol m^{-2} d^{-1}) is greater than the total Hg inputs from direct deposition (150 ± 14 pmol m^{-2} d^{-1}) indicating that the estuary is a net Hg source to the atmosphere. Comparing evasion of Hg(0) for the year 2000 calculated using the scheme developed by Nightingale et al. (*38*) (16.1 mol yr^{-1}, 334 pmol m^{-2} d^{-1}) used in our standard simulation to the low-end estimate (*42, 43*) from the model developed by Liss and Merlivat (*39*) (11.1 mol yr^{-1}, 230 pmol m^{-2} d^{-1}) shows a 30% decline in water column Hg(0) losses. Aqueous reduction of Hg(II) and subsequent evasion of Hg from seawater removes inorganic Hg that could potentially be converted to bioavailable MeHg. However, MeHg concentrations in seawater are

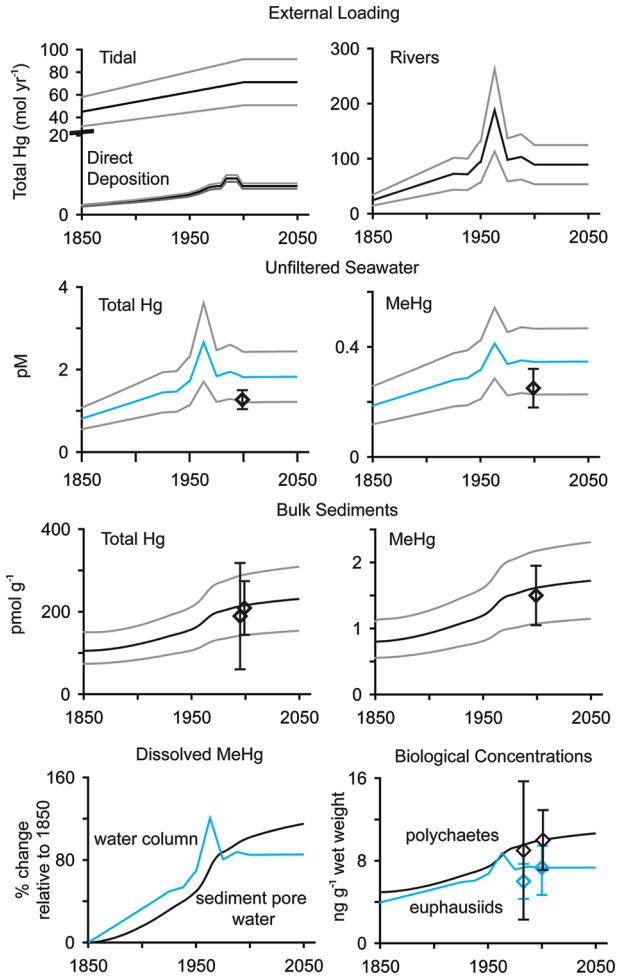

FIGURE 3. Reconstructed historical Hg loading to Passamaquoddy Bay between 1850 and 2000 and modeled changes in water, sediments, and biota. Constant loading is assumed between 2000 and 2050. Gray lines represent 95% confidence intervals around loading and concentrations based on measured variability in inputs from atmospheric deposition, rivers, and tides. Measured concentrations are shown as diamonds. Projected changes in polychaetes (biota sediment accumulation factor = 8.6×10^3) and euphausiids (bioaccumulation factor = 1.1×10^5) are calculated by assuming steady state with dissolved MeHg concentrations.

relatively insensitive to both the choice of evasion scheme and reduction rate coefficients. Model sensitivity analysis showed that a 60% increase in the water column Hg(II) reduction rate coefficient results in a less than 1% decline in MeHg concentrations in the year 2000 (SI Table S1). Similarly, the low (Liss and Merlivat) evasion estimates increase water column MeHg for the year 2000 by less than 1%.

For MeHg, tidal inflow represents the largest MeHg input into the water column due to large inflowing water volumes and a relatively high fraction of total Hg as MeHg (~24%) (Figure 2). Ambient MeHg concentrations that determine exposure of organisms will therefore be most affected by tidal inflow MeHg contributions. Primary producers take up 0.29 ± 0.21 mol MeHg yr^{-1} and 5.5 ± 1.7 mol Hg yr^{-1}, which is a small portion of water column fluxes on an annual basis (Figure 2). There is a net export of MeHg in tidal outflow of 4.5 ± 0.3 mol yr^{-1} or 93 ± 6 pmol m^{-2} d^{-1} (normalized to water surface area). Since fluxes of MeHg from the sediments to the water column through diffusion and resuspension are smaller than inputs from settling of suspended solids, MeHg inputs from rivers likely account for the majority of MeHg exported in tidal outflow. Other studies have suggested that the impacts of fluvial Hg discharges are limited to a relatively small geographical region surrounding the river mouth (*44*, *45*). Burial fluxes for the study site shown in Figure 1 illustrate the high rates of solids deposition around the mouth of the St. Croix river (the major freshwater tributary) but do not preclude offshore transport of MeHg since a substantial portion of MeHg inputs (>90%) is in the dissolved phase (Figure 2).

Relative Importance of Inputs from Rivers, Tides, and Atmospheric Deposition. Direct atmospheric deposition accounted for a small fraction of cumulative external loading between 1850 and 2000 (Hg: 4%; MeHg: 0.2%) compared to rivers (Hg: 53%; MeHg: 26%) and inflowing tidal waters (Hg: 43%; MeHg: 75%) (Figure 3). However, atmospheric deposition indirectly accounts for the majority of external inputs, because the watershed is much larger than the water surface area. Differences between atmospheric and fluvial AEFs for each year between 1850 and 2000 provide a first estimate of local watershed sources and suggest that approximately 78% of the cumulative loading from rivers is from atmospheric deposition transported through the catchment. Constraining the time required for atmospheric Hg to travel through different types of watersheds is therefore important for predicting temporal responses of estuaries to changes in Hg deposition (*14*).

Temporal Trends in Hg Concentrations. Figure 3 shows that water column Hg and MeHg concentrations in Passamaquoddy Bay peaked in the 1960s due to elevated discharges from local industry (pulp and paper mills) along the St. Croix river (*46*) and have declined substantially since this time. Water column Hg concentrations respond rapidly to changes in loading, requiring approximately 60 days to reach 95% of steady state. These relatively fast changes occur because the annual magnitude of Hg and MeHg flows out of the water column exceeds the size of water column reservoirs resulting in rapid turnover (Figure 2).

The deep active sediment layer in Passamaquoddy Bay exacerbates slow changes in sediment and benthic food web concentrations. Approximately 200 years are required for sediment Hg and MeHg concentrations to reach 95% of steady state. More than 90% of the total mass of Hg and MeHg is contained in the sediment compartment (Figure 2). Fluxes of Hg and MeHg through resuspension, diffusion, burial, and particle settling are small compared to the reservoirs in benthic sediments (Figure 2), explaining why sediment concentrations respond much more slowly than the water column to changes in external loading. Concentrations of Hg and MeHg in benthic sediments reflect the integrated signal of inputs from the water column. Sensitivity analysis of model results (SI Figure S2) shows that the depth of the active sediment layer drives the temporal response of benthic sediments (e.g., steady state would be achieved in several decades if the active sediment layer depth was 1 cm rather than centuries for 15 cm (*4*)).

Dissolved pools of MeHg in water and sediments provide the best measure of available Hg at the base of pelagic and benthic food webs, respectively (*27*, *47*). Model simulations suggest that MeHg exposures and concentrations in pelagic biota have declined by almost 40% since their peak in the 1960s because of declines in water column concentrations (Figure 3). Figure 3 shows that MeHg concentrations in the water column and pelagic organisms are expected to remain stable at present emissions levels. In contrast, sediments and benthic organisms will gradually increase at a rate of 0.13% per year, which leads to a 6% increase by 2050 relative to 2000 levels. Even with substantial Hg emissions reductions achieved by national and international agreements benthic food web Hg concentrations will likely exhibit a long temporal lag before declines are achieved, while rapid and proportional declines in MeHg concentrations in the pelagic food web can be expected. Other estuaries with substantial tidal

resuspension and perturbation of benthic sediments can be expected to respond over time scales similar to those of Passamaquoddy Bay, while those with a shallower active sediment layer will respond more rapidly (SI Figure S2). Results presented here also suggest that water column and pelagic food web MeHg concentrations in estuaries with significant fluvial and tidal influx (short water residence times) will respond rapidly to changes in anthropogenic Hg loading.

Acknowledgments

We acknowledge financial support for this study from the National Science and Engineering Council of Canada (NSERC) Strategic Grants Program, the Gulf of Maine Council on the Marine Environment, and the Electric Power Research Institute. This work also benefited from field support and review from Raymond Cranston and Michael Parsons (Natural Resources Canada), Peter Wells (Environment Canada), Hugh Akagi, Gareth Harding, Tim Milligan, and Dave Wildish (Fisheries and Oceans, Canada) and Chris Knightes (U.S. EPA). Any use of trade, product, or firm names in this publication is for descriptive purposes only and does not imply endorsement by the U.S. Government. We thank five anonymous reviewers for helpful suggestions.

Note Added after ASAP Publication

Due to a production error, this paper published ASAP February 1, 2010 without the Acknowledgments section; the corrected version published ASAP February 8, 2010.

Supporting Information Available

Additional information on model sensitivity analysis, field data used to parametrize model, differential equations, and derivation of model rate coefficients are available in the Supporting Information.This material is available free of charge via the Internet at http://pubs.acs.org.

Literature Cited

(1) Clarkson, T.; Magos, L. The toxicology of mercury and its chemical compounds. *Crit. Rev. Toxicol.* **2006**, *36*, 609–662.

(2) Sheuhammer, A.; Meyer, M.; Sandheinrich, M.; Murray, M. Effects of environmental methylmercury on the health of wild birds, mammals, and fish. *Ambio* **2007**, *36* (1), 12–18.

(3) Sunderland, E. M. Mercury exposure from domestic and imported estuarine and marine fish in the U.S. seafood market. *Environ. Health Perspect.* **2007**, *115* (2), 235–242.

(4) Sunderland, E. M.; Gobas, F. A. P. C.; Heyes, A.; Branfireun, B. A.; Bayer, A. K.; Cranston, R. E.; Parsons, M. B. Speciation and bioavailability of mercury in well-mixed estuarine sediments. *Mar. Chem.* **2004**, *90*, 91–105.

(5) Hammerschmidt, C. R.; Fitzgerald, W. F. Geochemical controls on the production and distribution of methylmercury in near-shore marine sediments. *Environ. Sci. Technol.* **2004**, *38* (5), 1487–1495.

(6) Hollweg, T. A.; Gilmour, C. C.; Mason, R. P. Biogeochemical controls over methylmercury production in the mid-Atlantic coastal region. *Mar. Chem.* **2009**, *114*, 86–101.

(7) Mitchell, C. P. J.; Gilmour, C. C. Methylmercury production in a Chesapeake Bay salt marsh. *J. Geophys. Res.* **2008**, *113*, G00C04.

(8) NRC. *Toxicological Effects of Methylmercury*; National Academy Press: Washington, DC, 2000; p 368.

(9) Sunderland, E. M.; Chmura, G. L. An inventory of historical mercury pollution in Maritime Canada: Implications for present and future contamination. *Sci. Total Environ.* **2000**, *256* (1), 39–57.

(10) Sunderland, E. M.; Chmura, G. L. The history of mercury emissions from fuel combustion in Maritime Canada. *Environ. Pollut.* **2000**, *110*, 1–10.

(11) Harding, G.; Dalziel, J.; Vass, *Prevalence and bioaccumulaton of methylmercury in the food web of the Bay of Fundy, Gulf of Maine, 6th Bay of Fundy Workshop, Cornwallis, Nova Scotia, Canada*, September 29−2 October 2004; Percy, J. A., Evans A. J., Wells P. G., Rolston S. J., Eds.; Environment Canada, Atlantic Region: Cornwallis, Nova Scotia, Canada, pp 76−77.

(12) Burgess, N.; Evers, D.; Kaplan, J. Mercury and other contaminants in common loons breeding in Atlantic Canada. *Ecotoxicology* **2005**, *14*, 241–252.

(13) Kamman, N.; Lorey, P.; Driscoll, C. T.; Estabrook, R.; Major, A.; Pienta, B.; Glassford, E. Assessment of mercury in waters, sediments and biota of New Hampshire and Vermont lakes, USA, sampled using a geographically randomized design. *Environ. Toxicol. Chem.* **2004**, *23*, 1172–1186.

(14) Harris, R.; et al. Whole ecosystem study shows rapid fish-mercury response to changes in mercury deposition. *Proc. Natl. Acad. Sci. U.S.A.* **2007**, *104*, 16586–16591.

(15) Knightes, C.; Sunderland, E.; Barber, M.; Johnston, J.; Ambrose, R. J. Application of ecosystem scale fate and bioaccumulation models to predict fish mercury response times to chnages in atmospheric deposition. *Environ. Toxicol. Chem.* **2009**, *28* (4), 881–893.

(16) Sunderland, E. M.; Mason, R. Human impacts on open ocean mercury concentrations. *Global Biogeochem. Cycles* **2007**, *21*, GB4022.

(17) Rice, G. E.; Senn, D.; Shine, J. P. Relative importance of atmospheric and riverine mercury sources to the Northern Gulf of Mexico. *Environ. Sci. Technol.* **2009**, *43* (2), 415–422.

(18) Smith, G. J. D.; Jovellanos, C. L.; Gaskin, D. E. *Near-Surface Bio-Oceanographic Phenomena in the Quoddy Region, Bay of Fundy*; Report 1280; Canadian Fisheries and Aquatic Sciences: St. Andrews, N.B., June 1984; p 9.

(19) Gregory, D.; Petrie, B.; Jordan, F.; Langille, P. Oceanographic, geographic and hydrological parameters of Scotia-Fundy and southern Gulf of St. Lawrence inlets. *Can. Tech. Rep. Hydrogr. Ocean Sci.* **1993**, (143), 248.

(20) Gulf of Maine Council on the Marine Environment. *Marine Environmental Quality in the Gulf of Maine: Fact Sheet 94-1*; Gulf of Maine Council on the Marine Environment: Boston, MA, 1994; p 16.

(21) Sunderland, E.; Cohen, M.; Selin, N.; Chmura, G. Reconciling models and measurements to assess trends in atmospheric mercury deposition. *Environ. Pollut.* **2008**, *156*, 526–535.

(22) Dalziel, J.; Harding, G.; Sunderland, E., The mercury flux of an east coast marine embayment. *8th International Conference on Mercury as a Global Pollutant*; Madison, WI, August 6−11, 2006.

(23) Heyes, A.; Mason, R.; Kim, E.; Sunderland, E. Mercury methylation in estuaries: Insights from measuring rates using stable mercury isotopes. *Mar. Chem.* **2006**, *102*, 134–147.

(24) Sunderland, E. M.; Gobas, F. A. P. C.; Branfireun, B. A.; Heyes, A. Environmental controls on the speciation and distribution of mercury in coastal sediments. *Mar. Chem.* **2006**, *102*, 111–123.

(25) Loring, D. H.; Milligan, T. G.; Willis, D. E.; Saunders, K. S. *Metallic and Organic Contaminants in Sediments of the St. Croix Estuary and Passamaquoddy Bay*; Canadian Technical Report of Fisheries and Aquatic Sciences No. 2245: Dartmouth, N.S., 1998; p 38.

(26) Robinson, S. M. C.; Martin, J. D.; Page, F. H.; Losier, R. *Temperature and Salinity Characteristics of Passamaquoddy Bay and Approaches Between 1990−1995*; Canadian Technical Report of Fisheries and Aquatic Sciences No. 2139: St. Andrews, N.B., 1996.

(27) Hammerschmidt, C.; Fitzgerald, W.; Lamborg, C.; Balcom, P.; Visscher, P. Biogeochemistry of methylmercury in sediments of Long Island Sound. *Mar. Chem.* **2004**, *90*, 31–52.

(28) Mason, R. P.; Lawson, N. M.; Lawrence, A. L.; Leaner, J.; Lee, J. G.; Sheu, G.-R. Mercury in the Chesapeake Bay. *Mar. Chem.* **1999**, *65*, 77–96.

(29) Gobas, F. A. P. C.; Pasternak, J. P.; Lien, K.; Duncan, R. K. Development and field validation of a multimedia exposure model for waste load allocation in aquatic ecosystems: Application to 2,3,7,8-tetrachloro-p-dioxin and 2,3,7,8-tetrachlorodibenzofuran in the Fraser River watershed. *Environ. Sci. Technol.* **1998**, *32*, 2442–2449.

(30) Gobas, F. A. P. C.; Z'Graggen, M. N.; Zhang, X. Time response of the Lake Ontario ecosystem to virtual elimination of PCBs. *Environ. Sci. Technol.* **1995**, *29* (8), 2038–2046.

(31) Dalzeil, J. A.; Yeats, P. A.; Amirault, B. P. Inorganic chemical analysis of major rivers flowing into the Bay of Fundy, Scotian Schelf, and Bras d'Or Lakes. *Can. Tech. Rep. Fish. Aquat. Sci.* **1998**, *2226* (vii), 140.

(32) O'Reilly, J.; Evans-Zetlin, C.; Busch, D. Primary Production. In *Georges Bank*; Backus, R. H., Bourne, D. W., Eds.; MIT Press: Cambridge, MA, 1987; pp 220−233.

(33) Boudreau, B. P. The mathematics of early diagensis: from worms to waves. *Rev. Geophys.* **2000**, *38* (3), 389–416.

(34) Gill, G. A.; Bloom, N. S.; Cappellino, S.; Driscoll, C. T.; Dobbs, C.; McShea, L.; Mason, R.; Rudd, J. W. M. Sediment-water fluxes

of mercury in Lavaca Bay, Texas. *Environ. Sci. Technol.* **1999**, *33* (5), 663–669.
(35) Mason, R.; Bloom, N.; Cappellino, S.; Gill, G.; Benoit, J.; Dobbs, C. Investigation of porewater sampling methods for mercury and methylmercury. *Environ. Sci. Technol.* **1998**, *32* (24), 4031–4040.
(36) Cressie, N. A. C. *Statistics for Spatial Data*; John Wiley and Sons: New York, 1991.
(37) Press, W. *Numerical Recipes: The Art of Scientific Computing*; Cambridge University Press: Cambridge, UK, 1986.
(38) Nightingale, P.; Malin, G.; Law, C.; AJ, W.; Liss, P.; Liddicoat, M.; Boutin, J.; Upstill-Goddard, R. In situ evaluation of air-sea gas exchange parameterizations using novel conservative and volatile tracers. *Global Biogeochem. Cycles* **2000**, *14* (1), 373–387.
(39) Liss, P. S.; Merlivat, L., Air-sea exchange rates: Introduction and synthesis. In *The role of Air-Sea Exchange in Geochemical Cycling*; Buat-Menard, P., Ed.; D Reidel Publishing Company: Dodrecht, 1986; pp 113−127.
(40) Balcom, P. H.; Hammerschmidt, C. R.; Fitzgerald, W. F.; Lamborg, C. H.; O'Connor, J. S. Seasonal distributions and cycling of mercury and methylmercury in the waters of New York/New Jersey Harbor Estuary. *Mar. Chem.* **2008**, *109* (1−2), 1–17.
(41) Sunderland, E. M.; Krabbenhoft, D. P.; Moreau, J. W.; Strode, S. A.; Landing, W. M. Mercury sources, distribution, and bioavailability in the North Pacific Ocean: Insights from data and models. *Global Biogeochem. Cycles* **2009**, *23*, No. GB2010.
(42) Rolfhus, K.; Fitzgerald, W. F. The evasion and spatial/temporal distribution of mercury species in Long Island Sound, CT-NY. *Geochim. Cosmochim. Acta* **2001**, *65* (3), 407–418.
(43) Andersson, M. E.; Gardfeldt, K.; Wangberg, I.; Sprovieri, F.; Pirrone, N.; Lindqvist, O. Seasonal and daily variation of mercury evasion at coastal and off shore sites from the Mediterranean Sea. *Mar. Chem.* **2007**, *104* (3−4), 214–226.
(44) Rice, G. E.; Senn, D. B.; Shine, J. P. Relative Importance of Atmospheric and Riverine Mercury Sources to the Northern Gulf of Mexico. *Environ. Sci. Technol.* **2009**, *43* (2), 415–422.
(45) Cossa, D.; Martin, J.-M.; Takayanagi, K.; Sanjuan, J. The distribution and cycling of mercury species in the western Mediterranean. *Deep-Sea Res. II* **1997**, *44* (3−4), 721–740.
(46) Fink, L. K. J.; Pope, D. M.; Harris, A. B.; Schick, L. L. *Heavy Metal Levels in Suspended Particulates, Biota, and Sediments of the St. Croix Estuary in Maine*; Land and Water Resources Institute, University of Maine at Orono: Orono, ME, 1976; p 59.
(47) Mason, R. P.; Reinfelder, J. R.; Morel, F. M. Uptake, toxicity, and trophic transfer of mercury in a coastal diatom. *Environ. Sci. Technol.* **1996**, *30* (6), 1835–1845.

ES9032524

SUPPORTING INFORMATION

Response of a Macrotidal Estuary to Changes in Anthropogenic Mercury Loading between 1850 and 2000

Elsie M. Sunderland[†*], *John Dalziel*[‡], *Andrew Heyes*[§], *Brian A. Branfireun*[||], *David P. Krabbenhoft*[⊥], *Frank A.P.C. Gobas*[⌈]

[†]Harvard University, School of Engineering and Applied Sciences, Cambridge MA, 02138, USA

[‡]Environment Canada, Meteorological Service of Canada, 45 Alderney Drive, Dartmouth, Nova Scotia, B2Y 2N6, Canada

[§]Chesapeake Biological Laboratory, University of Maryland Center for Environmental Science, University System of Maryland, Solomons, MD, 20688, USA

[||]Department of Geography, University of Toronto at Mississauga, 3359 Mississauga Road North, Mississauga, Ontario, L5L 1C6, Canada

[⊥]U.S. Geological Survey, 8505 Research Way, Middleton, WI, 53562, USA

[⌈]School of Resource and Environmental Management, Simon Fraser University, Burnaby, British Columbia, V5A 1S6, Canada

Contents **Page(s)**

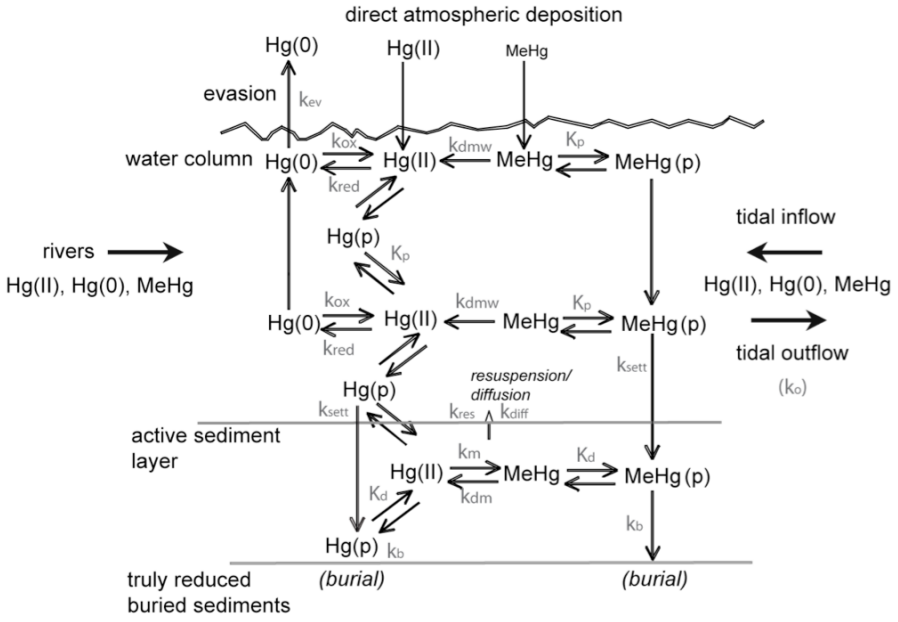

Figure S1. Conceptual diagram of Hg transport and transformation processes included in estuarine Hg cycling model.

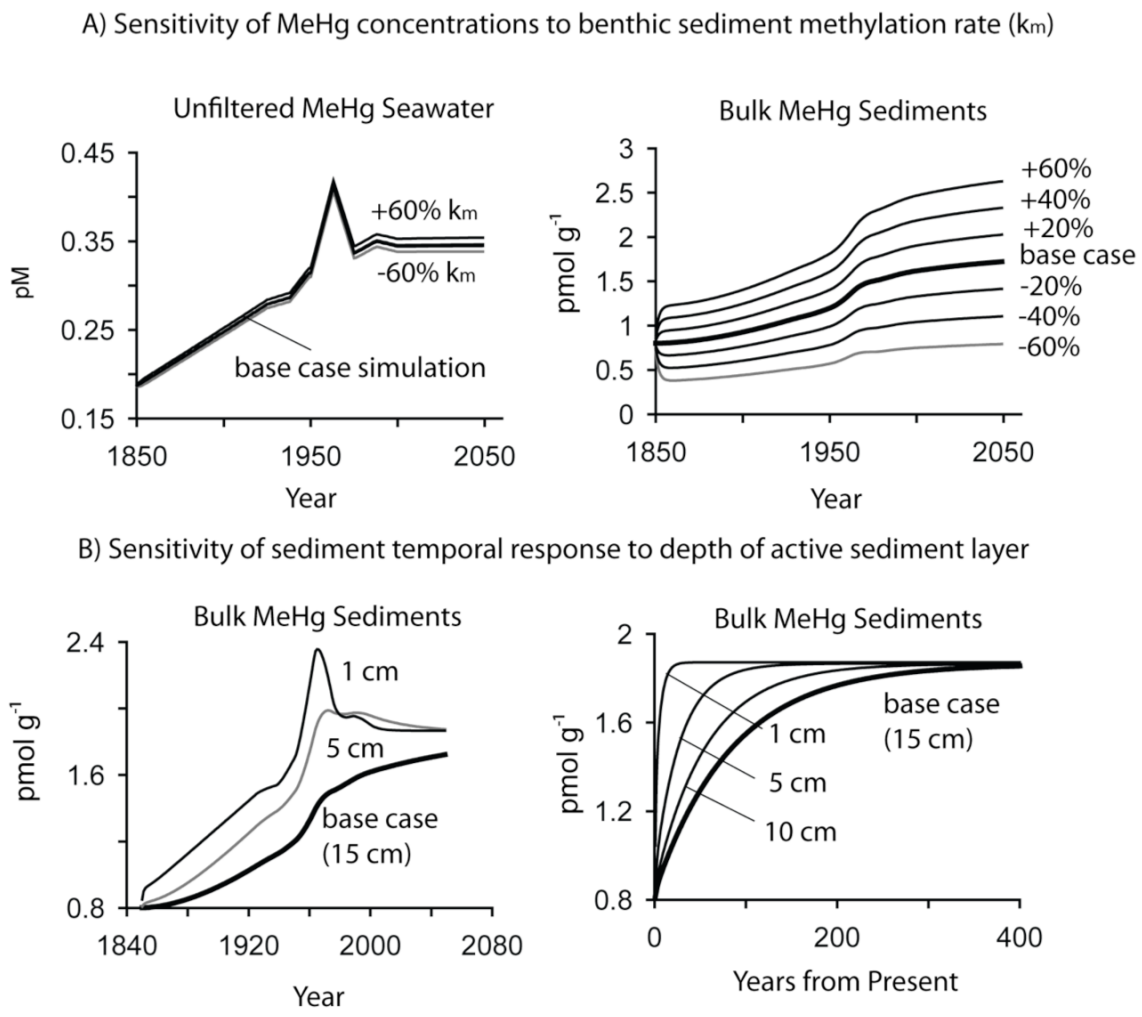

Figure S2. Selected model sensitivity analysis results. Panel (A) shows changes in sediment and water column MeHg concentrations with benthic sediment methylation rate changes. Panel (B) shows changes in the temporal response of benthic sediment MeHg concentrations with changes in the active sediment layer depth. Left panel shows historical simulation, while right panel shows changes in concentrations for 400 years simulated by forcing the model with present-day (ca. 2000) loadings.

Table S1. Sensitivity analysis of change in year 2000 seawater (C_w) MeHg concentrations with changes in the sediment methylation rate (k_m), and reduction rate (k_{red})

C_w MeHg	-60%	-40%	-20%	+20%	+40%	+60%
k_m	-2.14%	-1.45%	-0.72%	+0.69%	+1.39%	+2.08%
k_{red}	0.58%	0.35%	0.17%	-0.17%	-0.32%	-0.43%

Section I: Site-specific data

Table S2. Measured Hg concentration data.

Description	Mercury concentrations (mean±stdev)	
	Total Hg	MeHg
Benthic sediments		
Bulk sediments (pmol/g)	209±65	1.50±0.45
Interstitial water (pM)	70±33	4.4±2.5
Partition coefficient (log K_D, L/kg)	3.56±0.19	2.57±0.27
Potential methylation rate (d^{-1})	n/a	0.0264
Seawater (pM)		
June 2001 (n=10)	1.52±0.62	0.19±0.09
Nov. 2001 (n=4)	1.07±0.18	0.32±0.08
Aug. 2002 (n=8)	1.22±0.22	0.25±0.10
Partition coefficient (log K_P, L/kg)	5.61 (Hg(II))	4.35
Tidal Inflow (pM)		
Aug. 2000 (n=17)	1.21±0.29	n/a
June 2001 (n=29)	1.28±0.49	0.26±0.12
Aug. 2002 (n=26)	1.10±0.25	0.32±0.11
Atmospheric data		
[a]Total gaseous Hg (pmol m^{-3})	7.08	n/a
[a]Average wet deposition (nmol m^{-2} yr^{-1})	30.9±6.7	n/a
Total annual deposition (nmol m^{-2} yr^{-1})	54.8±0.5	0.50±0.35[b]
Rivers (pM)		
Magaguadavic (Nov.)	18.8±13.9	1.36
Magaguadavic (May)	22.1±4.0	1.58
Magaguadavic (Aug.)	8.7±3.9	n/a
Digdegaush (Nov.)	25.4±11.1	1.35
Digdegaush (May)	29.1±4.1	1.27
Digdegaush (Aug.)	7.8±3.0	n/a
St. Croix (Nov.)	20.2	0.68
St. Croix (May)	21.0±1.0	1.39
St. Croix (Aug.)	10.6±4.9	n/a

n/a = not available. Benthic sediment data are from Sunderland et al. *(1, 2)*. Seawater and river data are from Dalziel et al. *(3, 4)*. Partition coefficient for seawater is based on measured concentrations in phytoplankton *(5)*. Atmospheric data are from the Mercury Deposition Network (MDN) station NB-02 in St. Andrews, New Brunswick (45.0833N, 67.0833W) *(6, 7)*, Sunderland et al. *(8)*, and data from Environment Canada.

Seawater collection and analysis methods:

Sampling sites in Passamaquoddy Bay and the outer Bay of Fundy representative of tidal waters flowing into Passamaquoddy Bay were occupied on three expeditions from 2000 to 2002. The site locations were selected to sample the Scotian Shelf inflow to the Bay of Fundy and the deep-water inflow from Northeast Channel. Unfiltered water samples for both total and methyl mercury were collected using a General Oceanics Lever Action Niskin® modified for trace metal sampling. The Niskin modification involved Teflon - end caps, drain spout and internal coating. To further reduce the possibility of contamination, established clean sampling methods were employed *(9)*. Sub-sampling was carried out in a clean area of boat and the water collected for Hg drawn first from the Niskin. The water samples were collected into a precleaned Teflon bottles and double bagged until the samples could be preserved. Samples were preserved with 2 ml L^{-1} BrCl (total Hg) and 2 ml L^{-1} 9M H_2SO_4 (MeHg) within 2 hours of collection when the boat became stable or at dockside. All samples were analyzed in a dedicated mercury laboratory using EPA Methods 1631 for total Hg and 1630 for methyl Hg. For total Hg analysis, samples were digested at 60°C for 24 hours and if excess BrCl was not evident in the sample, additional BrCl was added and the heat-digestion step repeated. Methyl Hg samples were stored at -4 °C prior to analysis. Further Methods and detection limits (total Hg: 0.20 pM; MeHg 32 fM) for Passamaquoddy Bay samples were those described in Sunderland et al. *(1)* for aqueous samples.

Table S3. Summary of study-site characteristics.

Physical/Biological Properties	
Water surface area (m^2)	1.32×10^8
Sediment surface area (m^2)	1.48×10^8
Intertidal surface area (m^2)	1.54×10^7
Water volume (m^3)	2.81×10^9
Active sediment layer depth (m)	0.015
Sediment volume (m^3)	2.22×10^9
Average wind speed (m s^{-1}) (7 m above surface)	4.56±1.14
Average water depth (m)	30 m
Average water temperature (°C)	9
Average salinity (‰)	30
Net primary productivity (g C m^{-2} yr^{-1})	296
Average shortwave radiation intensity (W m^{-2})	211
Average daylight hours (St. Andrews, NB)	12.21
Shortwave radiation adj. for cloud cover and daylight (W m^{-2})	70
Hydrologic Properties	
Seawater outflow (m^3 yr^{-1})	6.41×10^{10}
Precipitation inputs (average 1996-2004, m^3 yr^{-1})	1.41×10^8
Freshwater inflow into estuary (m^3 yr^{-1})	4.68×10^9
Flushing time (days)	16
Tidal inflow (m^3 yr^{-1})	5.92×10^{10}
Solids Characteristics	
Water column suspended solids concentration (kg L^{-1})	1.76×10^{-6}
Suspended solids density (kg L^{-1})	1.5
Organic carbon content of suspended solids (unitless)	0.14±0.05
Median suspended solids particle diameter (μm)	5.0
Solids concentration in benthic sediment (kg L^{-1})	0.67
Benthic sediment solids density (kg L^{-1})	2.65
Tidal waters suspended solids concentration (kg L^{-1})	3.67×10^{-6}
Freshwater inflow suspended solids concentration (kg L^{-1})	3.40×10^{-6}
Benthic sediments organic carbon content (unitless)	0.018±0.006
Basin-wide average burial rate of benthic sediments (cm yr^{-1})	0.082
Intertidal sediment burial rate (cm yr^{-1})	0.55 (0.37-0.65)
Intertidal sediment bulk density (kg L^{-1})	0.57 (0.49-0.64)

Physical data from: Gregory et al. *(10)*, Sunderland et al. *(2)*, Robinson et al. *(11)*, and (GoMOOS JO2: http://www.gomoos.org/gnd); *Hydrologic* data from: Gregory et al. *(10)* and Ketchum and Kern *(12)* and average precipitation rate (1.065 m yr^{-1}) measured at St. Andrews, NB (45.09°N 67.00°W) between 1996-2004 *(6, 7)*; *Solids balance* data from: Sunderland et al. *(1, 2)*, Showell and Gaskin *(13)*, Dalziel et al. *(3, 4)*, Gobas et al. *(14)* and Hung and Chmura *(15)*.

Section II: Differential equation for total Hg, Hg(0), Hg(II), and MeHg

Total Mercury

For total Hg, the model simulates time-dependent (t) changes in the water (M_w, mol) and sediments (M_s, mol) reservoirs as follows:

$$\frac{dM_w}{dt} = (A + R + T) + (k_{res} + k_{diff})M_s - (k_{ev} + k_o + k_{sett})M_w$$

$$\frac{dM_s}{dt} = k_{sett}M_w - (k_{res} + k_{bur} + k_{diff})M_s$$

Where,

A = atmospheric deposition (mol d^{-1})
R = river discharges (mol d^{-1})
T = tidal inflow (mol d^{-1})
k_{res} = rate coefficient for benthic solids resuspension (d^{-1})
k_{diff} = rate coefficient for sediment-to-water diffusion of Hg(II) and MeHg (d^{-1})
k_{ev} = rate coefficient for evasion of Hg(0) from the water column (d^{-1})
k_o = rate coefficient for seawater outflow (d^{-1})
k_{sett} = rate coefficient for settling of suspended particles (d^{-1})
k_{bur} = rate coefficient for burial of benthic solids (d^{-1})

Hereon, for each major form of Hg, we denote total external loading of dissolved and particulate phase Hg as "*L*" (mol d^{-1}).

Methylmercury (MeHg)

Water column:

$$\frac{dM_{wMeHg}}{dt} = L_{MeHg} + (k_{res(MeHg)} + k_{diff(MeHg)})M_{sMeHg} - (k_{o(MeHg)} + k_{sett(MeHg)} + k_{dmw})M_{wMeHg}$$

Benthic sediments:

$$\frac{dM_{sMeHg}}{dt} = k_{sett(MeHg)}M_{wMeHg} - (k_{res(MeHg)} + k_{bur(MeHg)} + k_{diff(MeHg)})M_{sMeHg} - k_{dm}M_{sdMeHg} + k_m M_{sdHgII}$$

Where,

k_m = rate coefficient for methylation (d^{-1})
k_{dm} = rate coefficient for demethylation (d^{-1})
M_{sd} = dissolved reservoir of Hg in benthic sediments, used as a proxy for the bioavailable pools for methylation and demethylation. The dissolved pool is calculated at each time step in the simulation based on empirically measured partition coefficients (K_d) for MeHg and Hg(II) *(1, 2)*.

Elemental Mercury (Hg(0))

Water column:

$$\frac{dM_{wHg0}}{dt} = L_{Hg0} + k_{red}\phi M_{wHgII} - (k_{o(Hg0)} + k_{ev(Hg0)} + k_{ox})M_{wHg0}$$

Where,

k_{ox} = rate coefficient for oxidation of Hg(0) in the water column. We include terms for both photo-oxidation *(16)* and dark oxidation *(17, 18)* in the overall oxidation rate.

k_{red} = rate coefficient for reduction of Hg(II) in the water. Terms for photolytic and biotic reduction *(16, 19)* are included in the overall reduction rate.

ϕ = fraction of Hg(II) in the water column that is reducible.

Benthic sediments:

We do not include Hg(0) in benthic sediments because there are no data on Hg(0) concentrations in marine sediments.

Divalent mercury (Hg(II))

Water column:

$$\frac{dM_{wHgII}}{dt} = L_{HgII} + (k_{sw(HgII)} + k_{diff(HgII)})M_{sHgII} - (k_{o(HgII)} + k_{ws(HgII)} + k_{red})M_{wHgII}$$
$$+k_{dm}M_{sdMeHg} + k_{dmw}M_{wMeHg} + k_{ox}M_{wHg(0)}$$

Benthic sediments:

$$\frac{dM_{sHgII}}{dt} = k_{ws(HgII)}M_{wHgII} - (k_{sw(HgII)} + k_{diff(HgII)} + k_{b(HgII)})M_{sHgII} + k_m M_{sdHgII} + k_{dm}M_{sdMeHg}$$

Section III: External loading from rivers, tides and atmospheric deposition

Rivers

Table S4. Cumulative freshwater discharges (m^3 mo^{-1} x 10^8) into Passamaquoddy Bay reported by Gregory et al. *(10)*.

Winter			*Spring*			*Summer*			*Fall*		
Jan	Feb	Mar	Apr	May	Jun	Jul	Aug	Sept	Oct	Nov	Dec
3.34	3.03	4.32	8.82	6.37	3.51	2.54	2.21	2.06	2.78	3.68	4.12
Percent discharge by season:											
22.9%			40.0%			14.5%			22.6%		

The three major freshwater tributaries flowing into Passamaquoddy Bay are the Digdegaush (13.1%), Magaguadavic (25.2%) and St. Croix Rivers (61.7%) *(20)*. Solids and dissolved phase inputs were determined based on the suspended solids concentrations and partition coefficients for Hg(II) and MeHg derived from the particulate organic carbon content of suspended solids *(13)*. Concentrations of suspended particulate matter measured in freshwater discharges ranged between 1.19 and 6.19 mg $L^{-1}$with a weighted annual average concentration of suspended particulates of 3.43±1.03 mg L^{-1}

Historical Loading

We calculate historical loading by applying anthropogenic enrichment factors (AEFs) from sediment records (for atmospheric and fluvial inputs) *(2, 8)* and a linear extrapolation of anthropogenic enrichment modeled in the North Atlantic Ocean *(21)*. We divide measured inputs (ca. 2000) by the AEF for 1850 and then extrapolate results to intermediate years using the AEF corresponding to each year. We calculate upper and lower 95% confidence intervals for loading based on the measured variability in year 2000 inputs. We interpolate between years assuming a linear rate of change in loading.

Speciation

Table S5. Speciation of loading from tides, rivers and atmospheric deposition. For all simulations, speciation of Hg in inputs assumed to be constant based on measured concentrations of total Hg and MeHg. High, mean and low estimates are based on variability in the measured data.

	MeHg	Hg(0)	Hg(II)
	Atmospheric deposition		
Mean	0.9%	n/a	99.1%
Low 95% CI	0.2%	n/a	99.8%
High 95% CI	1.4%	n/a	98.6%
	Fluvial inputs		
Mean	6.5%	10.0%	83.6%
Low 95% CI	5.6%	10.0%	84.4%
High 95% CI	8.6%	10.0%	81.4%
	Tidal inputs		
Mean	24.3%	13.0%	62.8%
Low 95% CI	20.7%	7.0%	72.3%
High 95% CI	26.3%	19.0%	54.7%

n/a = not applicable. Net flux of Hg(0) is modeled explicitly in the derivation of the evasion rate coefficient (see section IV). Based on Amyot et al. *(22)*, we assume that Hg(0) is 10% of the total loading.

Section IV: Derivation of model rate coefficients

Table S6. Summary of model rate coefficients for year 2000 simulation (d^{-1}). Descriptions of methods and data used to derive each rate constant are provided below.

Process	Rate Coefficients
Seawater outflow	$k_o = 0.0625$
Evasion of Hg(0)	$k_{ev} = 0.0490$
Solids settling Hg(II)	$k_{sett} = 0.0402$
Solids resuspension Hg(II)	$k_{res} = 9.74 \times 10^{-6}$
Burial Hg(II)	$k_{bur} = 2.38 \times 10^{-5}$
Sediment-to-water diffusion Hg(II)	$k_{diff} = 1.55 \times 10^{-6} – 7.33 \times 10^{-6}$
Benthic sediment methylation	$k_m = 0.0264$
Benthic sediment demethylation	$k_{dm} = 0.34$
Solids settling MeHg	$k_{sett(MeHg)} = 0.0036$
Photodecomposition of MeHg in water	$k_{dmw} = 0.0015$
Solids resuspension MeHg	$k_{res} = 9.70 \times 10^{-6}$
Burial MeHg	$k_{bur(MeHg)} = 2.37 \times 10^{-5}$
Sediment-to-water diffusion MeHg	$k_{diff(MeHg)} = 1.55 \times 10^{-5} – 9.14 \times 10^{-5}$
Photo-oxidation of Hg(0) in water	$k_{ox1} = 0.6081$
Photo-reduction of Hg(II) in water	$k_{red1} = 0.6408$
Dark oxidation of Hg(0) in water	$k_{ox2} = 0.4840$
Biotic reduction of Hg(II) in water	$k_{red2} = 0.0287$

Sediment burial

Benthic sediment burial rates were measured using vertical gradients of dissolved ammonium and sulfate in gravity cores collected at multiple stations (n=20) following the method developed by Cranston *(23, 24)*. Details of sampling and analytical techniques are reported in Sunderland et al. *(2)*. The intertidal area was calculated from the difference between water surface area at low and high tide from Gregory et al. *(10)* and accounts for 10% of the total sediment surface area in the Bay.

The coefficient for sediment burial (k_b) is based on burial rates measured in gravity cores collected at multiple stations (n=27) *(2)*. For the main bay, we constructed a spatial grid of sediment accumulation using Kriging as a spatial interpolation method and estimated annual sediment burial across the system by summing volume estimates for each cell defined in the spatial grid (see burial flux diagram Figure 1). We also include sediment burial in intertidal mudflats based on measured Hg concentrations and accumulation rates reported in Hung and Chmura *(15)*. The total burial flux is the sum of burial in intertidal areas and the main bay. We divide this total flux by the surface area of the sediments to calculate an average basin wide burial rate (v_b, m d^{-1}), which we assume to be constant between 1850 and 2050. Rate coefficients for sediment burial of Hg(II) and MeHg (k_b, d^{-1}) are calculated from v_b, the sediment surface area (SA_{sed}, m^2), the sediment volume (V_{sed}, m^3), and the fraction of Hg(II) or MeHg in the dissolved phase of benthic sediments, as follows:

$$k_{bur} = SA_{sed} \bullet v_b \bullet (1 - f_{diss(sed)}) / V_{sed}$$

The $f_{diss(sed)}$ is based on the empirically measured partition coefficients for Hg(II) and MeHg in benthic sediments (K_D, L kg^{-1}, Table S2) and the concentrations of solids in benthic sediments (C_{ss}, kg L^{-1}):

$$f_{diss(sed)} = \frac{1}{(1 + K_D C_{SS})}$$

Settling of suspended solids

Rate coefficients for settling ($k_{ws,}$ d^{-1}) of Hg(II) and MeHg are based on the particle settling velocity (v_s, m d^{-1}), water surface area (SA_W, m^2), water volume ($V_{w,}$ m^3), and the fraction of dissolved Hg(II) or MeHg in the water column (f_{diss}, dimensionless):

$$k_{sett} = SA_W \bullet v_s \bullet (1 - f_{diss}) / V_w$$

where f_{diss} is the calculated from the empirically measured particle-water partition coefficient (K_P, L kg^{-1}) and the concentration of suspended solids in the water column (SPM, kg L^{-1}):

$$f_{diss} = \frac{1}{(1 + K_P SPM)}$$

Particle size spectra of nepheloid layer sediments were measured by the Particle Dynamics Laboratory at the Bedford Institute of Oceanography using Coulter analysis *(25)* at 24 stations in Passamaquoddy Bay in August 2000. Median particle diameter was determined to be 5 μm based on this analysis, which we use to calculate the average settling velocity of particles.

We calculate the average settling velocity for particles (v_s) based on the measured mean particle diameter and Stoke's law for particles falling in a viscous fluid *(26)*:

$$v_s = \frac{2}{9} \frac{(d_{pw} - d_{sw})}{\mu} g r_{pw}^{\ 2}$$

v_s = settling velocity of suspended solids (m s^{-1})
d_{pw} = density of suspended particles in seawater (kg m^{-3})
d_{sw} = density of seawater (kg m^{-3})
μ = dynamic viscosity of seawater (Pa s^{-1})
g = gravitational acceleration (m s^{-2})
r_{pw} = average radius of suspended solids (m)

Figure S3. Summary of particle size distributions

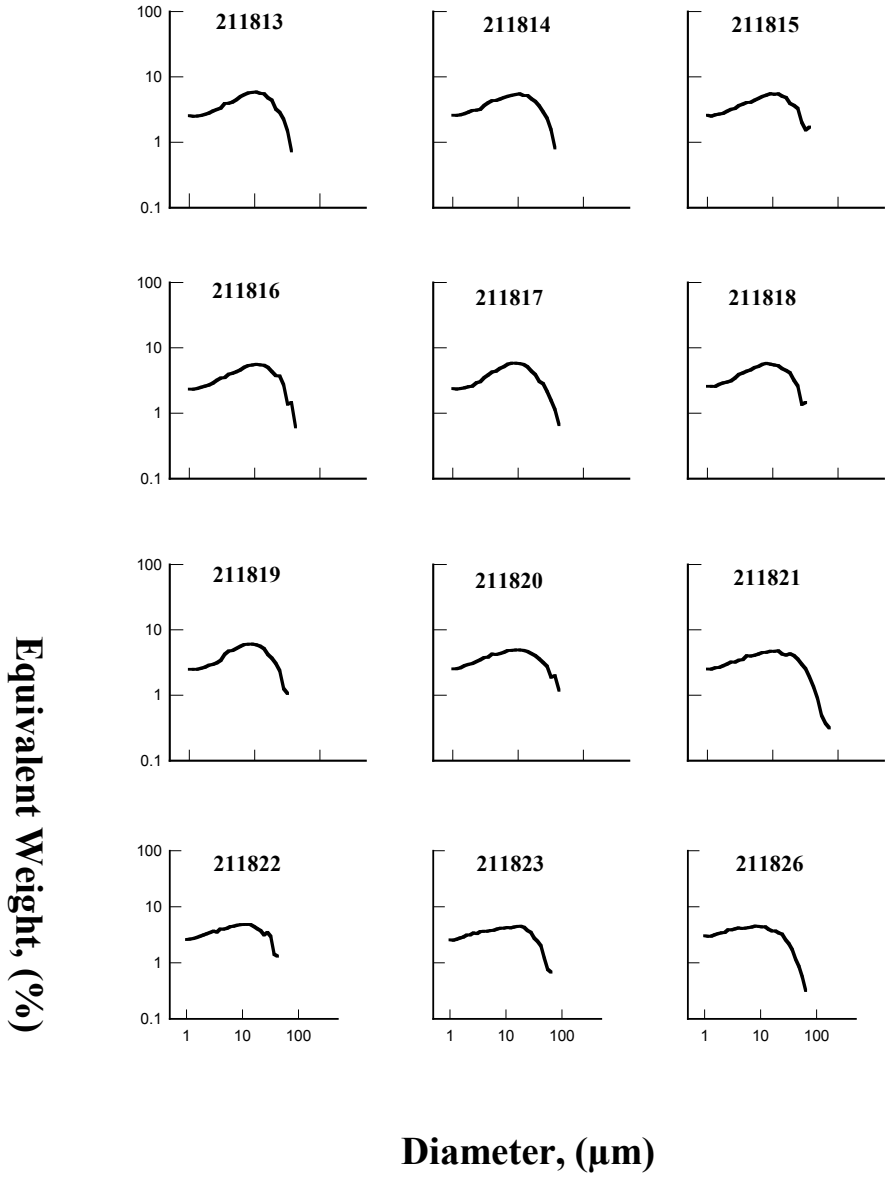

Particle Dynamics Lab, BIO

Solids resuspension

Rate coefficents for resuspension (k_{sw}, d^{-1}) of Hg(II) and MeHg are calculated as follows:

$$k_{res} = \mathrm{Re}\, sFlux / C_{ss} \bullet (1 - f_{diss(sed)}) / 1000 V_{sed}$$

where we assume that the solids resuspension flux (*ResFlux*) is equal to the difference between the settling and burial fluxes of solids (kg) *(14)*.

Sediment-to-water diffusion

Rate coefficients for diffusive fluxes of Hg(II) and MeHg from sediments into the water are calculated by dividing fluxes by the respective reservoirs of Hg species at each time step in the model simulation. Diffusional fluxes (*F*) of total Hg and MeHg are based on the parameterization described in Gill et al. *(27)* and Hammerschmidt et al. *(28)* and Fick's first law:

$$F = -\left(\frac{\varphi D_w}{\theta^2}\right)\frac{dC}{dx}$$

where F is the flux of solute (pmol m^{-2} d^{-1}); dC is the maximum concentration gradient of Hg species between depths (dx) and is assumed to be in the top 1 cm of the sediments; φ is the measured sediment porosity (0.74); θ is tortuosity ($1-\ln(\varphi^2)$); and D_w is the diffusion coefficient of the solute in water.

We model high and low ranges of diffusional fluxes for Hg(II) and MeHg using diffusion coefficients (cm^2 s^{-1}) calculated for different Hg species-complexes in sediment pore waters at 25°C. To calculate a lower bound for both Hg(II) and MeHg diffusion, we use a diffusion coefficient of $D_w = 2.0 \times 10^{-6}$, which was derived for macromolecular organic matter in the colloidal size range *(27)*. As an upper bound, we use diffusion coefficients of $D_w = 1.2 \times 10^{-5}$ *(28)* for MeHg and $D_w = 9.5 \times 10^{-6}$ *(27)* for Hg(II) based on CH_3HgSH^0 and $HgCl_4^{2-}$, respectively. Although other studies have suggested these species may not be the dominant complexes in porewaters, diffusion coefficients vary at most by a factor of two (T. Hollweg, UConn., PhD thesis) and thus the values for D_w chosen here are suitable for bounding high and low extremes of potential fluxes.

We calculate a temperature corrected diffusion coefficient based on the annual average water temperature of Passamaquoddy Bay (Table S3):

$$D_{w(T)} = D_{w(25)}/(1 + 0.048 \bullet (25 - T))$$

Methylation and demethylation rates

Methylation rate coefficients are based on measurements in sediment cores spiked with stable Hg(II) isotopes *(2, 29)* (Table S2). A detailed description of the experimental design and rate calculations can be found in Heyes et al. *(29)*. This method assumes that the added isotope is representative of the bioavailable pool of Hg(II), and that substantial depletion did not occur during the assay period. Spike concentrations were kept low (10-20% of in situ concentrations) to minimize the potential increase in Hg bioavailability with Hg(II) addition. Heyes et al. *(29)* showed across several estuaries that MeHg concentration is a good predictor of net methylation activity and that changes in MeHg concentrations are driven more by differences in the methylation rate than the demethylation rate. Heyes et al. *(29)* further hypothesized that the MeHg demethylation experiments actually underestimate MeHg demethylation compared to ratios Hg to MeHg concentrations in field samples, because a) the assumption of the back reaction of methylation is unimportant was not valid or b) some of the added MeHg becomes unavailable for demethylation over time. We also hypothesized that methylation and demethylation likely occur in similar zones of microbial activity thus newly methylated Hg maybe the most available for demethylation.

We therefore calibrated the demethylation rate to ensure that the ratio of methylation to demethylation matched the seasonally averaged measured percent MeHg in interstitial water. The fraction of total Hg present as MeHg in estuarine sediments has been shown to be a reliable indicator of net methylation in a variety of studies *(2, 28, 29)*. We use the dissolved pools of Hg(II) and MeHg in sediment pore waters as the bioavailable pool subject to microbial processes resulting in methylation and demethylation *(30)*.

We do not include *in situ* water column methylation because this system does not have the low oxygen conditions required to support net methylation *(32, 33)*.

Seawater outflow

The rate coefficient for seawater outflow (d^{-1}) of all species is the ratio of seaward flow to the estuarine volume and is based on the tidal flushing rate and the associated annually averaged daily net translocation of tidal water *(12)*. Ketchum and Keen *(12)* estimated the flushing time to be 16 days based on salinity measurements and freshwater inputs. The net volume of seaward flow (T_o) is estimated from this flushing time, which represents the length of time required for the estuary to exchange its volume (i.e., V_w/T_o = flushing time; where, V_w represents the average water volume of the estuary).

Photodecomposition of water column MeHg

The photodecomposition rate of MeHg in the water column is parameterized based on average shortwave radiation penetration in the water column (*RAD*, W m^{-2}), using data from Sellers et al. *(31)* ($k_{dmw} = 8.52 \times 10^{-4}$ x RAD). This relationship was derived in freshwater environments and is therefore highly uncertain when applied to marine seawater. However, bounding of photodecomposition based on the rate information provided in Sellers et al. *(31)* suggests that photodecomposition is a negligible component of water column MeHg losses on an annual basis (see Figure 2 main text). Methods and data used to calculate light attenuation in the water column are provided in Tables S3 and S7.

Oxidation and reduction rates

To characterize inorganic Hg redox reactions in the water column, we use dual isotope addition data from Whalin et al. *(16),* who confirmed that Hg oxidation (k_{ox}) and reduction (k_{red}) reactions occur simultaneously in seawater. We parameterize photo- reduction and oxidation as a function of total shortwave radiation and biotic reduction as a function of net primary productivity. By least-squares fit to rates reported in Whalin et al. *(16)*, we derived relationships between photoreduction, photoxidation and total shortwave radiation. Similarly, we derived from these data a relationship between the biotic reduction rate and productivity using values for the outer and shelf region of Chesapeake Bay characteristic of the measurement period *(34)*. We assume that the reducible pool of water column Hg(II) is 50% based on data showing colloidally bound species can account for >50% of Hg(II) in coastal waters and chloride complexes in marine waters may be more resistant to reduction *(16, 35)*.

We calculated an average light intensity throughout the water column of Passamaquoddy Bay using the local shortwave radiation flux and light attenuation based on spectral light absorption/scattering coefficients for seawater, DOC and pigments, and their respective

concentrations. Spectral light absorption coefficients listed below are from from the EXAMS model (see: http://www.epa.gov/ceampubl/swater/exams/index.html). We also include dark oxidation of Hg(0) based on Lalonde et al. *(17, 18)*.

Table S7. Summary of model parameters used to calculate oxidation of Hg(0) and reduction of Hg(II) in the water column.

Parameter	Description	Formulation
k_{ox1} (d^{-1})	photo-oxidation rate constant	$0.354 \bullet RAD$ *(16)*
k_{ox2} (d^{-1})	dark oxidation rate constant	0.484 *(17, 18)*
k_{red1} (s^{-1})	photolytic reduction rate constant	$0.373 \bullet RAD$ *(16)*
k_{bio} (s^{-1})	biotic reduction rate constant	$3.54 \times 10^{-2} \bullet NPP$ *(16)*
RAD_i (W m^{-2})	total local shortwave radiation penetration in the mixed layer	$\frac{1}{x_2 - x_1} \bullet \frac{RAD}{\eta}[e^{\eta x1} - e^{-\eta x2}]$
RAD (W m^{-2})	average annual shortwave radiation at the water surface	70
x_1 (m)	surface depth	0 m
x_2 (m)	average water depth	30 m
η (m^{-1})	extinction coefficient for radiation	$\eta_{water} + \eta_{Chl} C_{Chl} + \eta_{DOC} C_{DOC}$
η_{water} (m^{-1})	extinction coefficient for water	0.0145 (450 nm)
η_{Chla} (m^{-1})	extinction coefficient for pigments	31 (450 nm)
C_{Chla} (mg L^{-1})	average concentration of Chl a in mixed layer	0.65 x 10^{-3} *(13)*
η_{DOC} (mg L^{-1})	extinction coefficient for dissolved organic carbon (DOC)	0.654 (450 nm)
C_{DOC} (mg L^{-1})	average DOC concentrations in water column	2.0 *(36)*
NPP (gC m^{-2} d^{-1})	average annual net primary productivity	0.81 *(36)*

Evasion of Hg(0)

We model air-sea exchange of Hg(0) using the evasion scheme developed by Nightingale et al. *(37)* (referred to as 'N00' in Table S8) and wind speed data from a nearby (44°53'21" N, 67°00'44"W) Gulf of Maine Ocean Observing Station (GoMOOS JO2: http://www.gomoos.org/gnd). We compared this evasion flux to the scheme developed by Liss and Merlivat *(38)* (L&M86).

Total gaseous atmospheric Hg data are from MDN measurements in St. Andrews, NB *(6, 7)*, and water column Hg(0) concentrations are based on redox reaction rates. We use the temperature corrected Henry's Law constant for Hg(0) in seawater *(39)*, a temperature corrected Schmidt number for CO_2 *(40)*, and the temperature and salinity specific kinematic viscosity and diffusivity for Hg(0) calculated using the Wilke-Chang method *(41)*.

Table S8. Summary of parameters used to calculate air-sea exchange of Hg(0)

Parameter	Description	Formulation
F_v (nmol m^{-2} d^{-1})	Hg(0) air-sea exchange flux	$F_v = K_w(C_w - C_a / H'(T))$
C_w (pM)	concentration of Hg(0) in seawater	See differential equations
C_a (ng m^{-3})	concentration of Hg(0) in air	Mean MDN data NB-02 (Table S2)
H'(T)	Temperature dependent dimensionless Henry's law constant from Andersson et al. *(39)*	$\ln H' = (\frac{-2403.3}{T} + 6.92)$
T′ (ºC)	average water temperature	9 *(11)*
T (K)	water temperature in Kelvin	273 + T′
K_w (cm hr^{-1}) (N00)	water-side mass transfer coefficient for steady winds	$0.25u_{10}^2(Sc/Sc_{CO_2})^{-0.5}$
K_w (m s^{-1}) (L&M 86)	water-side mass transfer coefficient	For u_{10} >3.6 <13: $2.8\times10^{-6} \bullet (5.9u_{10} - 49.3) \bullet (Sc/Sc_{CO_2})^{-0.5}$
u_{10} (m s^{-1})	wind speed normalized to 10 m above sea surface, where z = measurement height (7m) and u_z = wind speed at measurement height.	$u_{10} = \frac{10.4u_z}{\ln(z) + 8.1}$
Sc_{CO_2}	Schmidt number for CO_2	$0.11T'^2 - 6.16T' + 644.7$ *(40)*
$Sc_{Hg(0)}$	Schmidt number for Hg(0)	ν / D
ν (cm^2 s^{-1})	kinematic viscosity	N/ρ = $0.017e^{(-0.025T')}$ *(40)*
N (cP)	viscosity of water	$1.88\times10^{-3} - 0.04\times10^{-3}T'$
ρ (mg cm^{-3})	seawater density	1025
D (cm^2 s^{-1})	diffusivity (Wilke-Chang *(41)* method)	$\frac{7.4\times10^{-8}(\phi_w M_w)^{1/2}T}{\mathrm{N}V_B^{0.6}}$
M_w (g mol^{-1})	molecular weight of water	18.0
V_B (cm^3 mol^{-1})	molal volume of mercury at its normal boiling temperature	12.74 *(42)*
ϕ_w	solvent association factor	2.26 *(43)*

References

(1) Sunderland, E. M.; Gobas, F. A. P. C.; Branfireun, B. A.; Heyes, A., Environmental controls on the speciation and distribution of mercury in coastal sediments. *Mar. Chem.* **2006,** *102*, 111-123.

(2) Sunderland, E. M.; Gobas, F. A. P. C.; Heyes, A.; Branfireun, B. A.; Bayer, A. K.; Cranston, R. E.; Parsons, M. B., Speciation and bioavailability of mercury in well-mixed estuarine sediments. *Mar. Chem.* **2004,** *90*, 91-105.

(3) Dalzeil, J. A.; Yeats, P. A.; Amirault, B. P., Inorganic chemical analysis of major rivers flowing into the Bay of Fundy, Scotian Schelf, and Bras d'Or Lakes. *Canadian Technical Report of Fisheries and Aquatic Sciences* **1998,** *2226*, (vii), 140.

(4) Dalziel, J.; Harding, G.; Sunderland, E., The mercury flux of an east coast marine embayment. In *8th International Conference on Mercury as a Global Pollutant*, Madison, WI, USA, 2006.

(5) Harding, G.; Dalziel, J.; Vass, P. In *Prevalence and bioaccumulaton of methylmercury in the food web of the Bay of Fundy, Gulf of Maine*, 6th Bay of Fundy Workshop, Cornwallis, Nova Scotia, Canada, September 29–2 October 2004, 2004; Percy, J. A., Evans AJ, Wells PG, Rolston SJ, Ed. Environment Canada, Atlantic Region: Cornwallis, Nova Scotia, Canada, 2004; pp 76-77.

(6) Kellerhals, M., et al., Temporal and spatial variability of total gaseous mercury in Canada: results from the Canadian Atmospheric Mercury Measurement Network (CAMNet). *Atmos. Environ.* **2003,** *37*, 1003-1011.

(7) Temme, C.; Blanchard, P.; Steffen, A.; Banic, C.; Beauchamp, S.; Poissant, L.; Tordon, R.; Wiens, B., Trend, seasonal and multivariate analysis study of total gaseous mercury data from the Canadian atmospheric mercury measurement network (CAMNet). *Atmos. Environ.* **2007,** *41*, 5423-5441.

(8) Sunderland, E.; Cohen, M.; Selin, N.; Chmura, G., Reconciling models and measurements to assess trends in atmospheric mercury deposition. *Environ Poll* **2008,** *156*, 526-535.

(9) Gill, G.; Fitzgerald, W., Mercury in surface waters of the open ocean. *Global Biogeochem. Cy.* **1987,** *3*, 199-212.

(10) Gregory, D.; Petrie, B.; Jordan, F.; Langille, P., Oceanographic, geographic and hydrological parameters of Scotia-Fundy and southern Gulf of St. Lawrence inlets. *Canadian Technical Report of Hydrographic Ocean Sciences* **1993**, (143), 248.

(11) Robinson, S. M. C.; Martin, J. D.; Page, F. H.; Losier, R. *Temperature and Salinity Characteristics of Passamaquoddy Bay and Approaches Between 1990-1995*; Canadian Technical Report of Fisheries and Aquatic Sciences No. 2139: St. Andrews, N.B., 1996.

(12) Ketchum, B. H.; Keen, D. J., The exchange of fresh and salt waters in the Bay of Fundy and in Passamaquoddy Bay. *Journal of the Fisheries Research Board of Canada* **1953,** *10*, (3), 97-121.

(13) Showell, M. A.; Gaskin, D. E., Partitioning of cadmium and lead within seston of coastal marine waters of the western Bay of Fundy. *Archives of Environmental Contamination and Toxicology* **1992,** *22*, 322-333.

(14) Gobas, F. A. P. C.; Z'Graggen, M. N.; Zhang, X., Time response of the Lake Ontario ecosystem to virtual elimination of PCBs. *Environ Sci Technol* **1995,** *29*, (8), 2038-2046.

(15) Hung, G. A.; Chmura, G., Mercury accumulation in surface sediments of salt marshes in the Bay of Fundy. *Environ. Poll.* **2006,** *142*, 418-431.

(16) Whalin, L.; Kim, E.; Mason, R., Factors influencing the oxidation, reduction, methylation and demethylation of mercury species in coastal waters. *Mar. Chem.* **2007,** *107*, 278-294.

(17) Lalonde, J.; Amyot, M.; Kraepiel, A.; Morel, F., Photooxidation of Hg(0) in artificial and natural waters. *Environ. Sci. Technol.* **2001,** *35*, 1367-1372.
(18) Lalonde, J. D.; Amyot, M.; Orvoine, J.; Morel, F. M. M.; Auclair, J. C.; Ariya, P. A., Photoinduced oxidation of Hg-0 (aq) in the waters from the St. Lawrence estuary. *Environ. Sci. Technol.* **2004,** *38*, (2), 508-514.
(19) Rolfhus, K.; Fitzgerald, W. F., The evasion and spatial/temporal distribution of mercury species in Long Island Sound, CT-NY. *Geochim. Cosmochim. Ac.* **2001,** *65*, (3), 407-418.
(20) Pol, R. A. *Chemical Loadings (Exports) to the Bay of Fundy: A Framework for Concentrations and Exports from Atlantic Canada Rivers*; International Joint Commission: Windsor, ON, Canada, January 1996, 1996.
(21) Sunderland, E. M.; Mason, R., Human impacts on open ocean mercury concentrations. *Global Biogeochem. Cy.* **2007,** *21*, GB4022.
(22) Amyot, M.; Lean, D. R. S.; Poissant, L.; Doyon, M.-R., Distribution and transformation of elemental mercury in the St. Lawrence River and Lake Ontario. *Can. J. Fish. Aquat. Sci.* **2000,** *57 (Suppl. 1)*, 155-163.
(23) Cranston, R. E., Sedimentation rate estimates from sulfate and ammonia gradients. *Proceedings of the Ocean Drilling Program, Scientific Results* **1991,** *119*, 401-405.
(24) Cranston, R. E., Organic carbon burial rates across the Arctic Ocean from the 1994 Arctic Ocean Section expedition. *Deep Sea Research II* **1997,** *44*, (8), 1705-1723.
(25) Loring, D. H.; Milligan, T. G.; Willis, D. E.; Saunders, K. S. *Metallic and Organic Contaminants in Sediments of the St. Croix Estuary and Passamaquoddy Bay*; Canadian Technical Report of Fisheries and Aquatic Sciences No. 2245: Dartmouth, N.S., 1998; p 38.
(26) Knightes, C., Development and test application of SERAFM: A screening-level mercury fate model and tool for evaluating wildlife exposure risk for surface waters with mercury-contaminated sediments. *Environmental Software and Modelling* **2008,** *23*, 495-510.
(27) Gill, G. A.; Bloom, N. S.; Cappellino, S.; Driscoll, C. T.; Dobbs, C.; McShea, L.; Mason, R.; Rudd, J. W. M., Sediment-water fluxes of mercury in Lavaca Bay, Texas. *Environ. Sci. Technol.* **1999,** *33*, (5), 663-669.
(28) Hammerschmidt, C.; Fitzgerald, W.; Lamborg, C.; Balcom, P.; Visscher, P., Biogeochemistry of methylmercury in sediments of Long Island Sound. *Mar. Chem.* **2004,** *90*, 31-52.
(29) Heyes, A.; Mason, R.; Kim, E.; Sunderland, E., Mercury methylation in estuaries: Insights from measuring rates using stable mercury isotopes. *Mar. Chem.* **2006,** *102*, 134-147.
(30) Benoit, J. M.; Gilmour, C. C.; Heyes, A.; Mason, R. P.; Miller, C., Geochemical and biological controls over methylmercury production and degradation in aquatic systems. *ACS Symp. Ser.* **2003,** *835*, 262-297.
(31) Sellers, P.; Kelly, C. A.; Rudd, J. W. M.; MacHutchon, A. R., Photodegradation of methylmercury in lakes. *Nature* **1996,** *380*, 694.
(32) Eckley, C. S.; Hintelmann, H., Determination of mercury methylation potentials in the water column of lakes across Canada *Sci. Tot. Environ.* **2006,** *368*, 111-125.
(33) Sunderland, E. M.; Krabbenhoft, D. P.; Moreau, J. W.; Strode, S. A.; Landing, W. M., Mercury sources, distribution, and bioavailability in the North Pacific Ocean: Insights from data and models. *Global Biogeochem. Cy.* **2009,** *23*, 14.
(34) Cerco, C., Phytoplankton kinetics in the Chesapeake Bay Eutrophication Model. *Water Quality and Ecosystem Modeling* **2000,** *1*, 5-49.
(35) Guentzel, J. L.; Landing, W. M.; Gill, G. A.; Pollman, C. D., Processes influencing rainfall deposition of mercury in Florida. *Environ. Sci. Technol.* **2001,** *35*, (5), 863-873.

(36) O'Reilly, J.; Evans-Zetlin, C.; Busch, D., Primary Production. In *Georges Bank*, Backus, R. H.; Bourne, D. W., Eds. MIT Press: Cambridge, MA, 1987; pp 220-233.
(37) Nightingale, P.; Malin, G.; Law, C.; AJ, W.; Liss, P.; Liddicoat, M.; Boutin, J.; Upstill-Goddard, R., In situ evaluation of air-sea gas exchange parameterizations using novel conservative and volatile tracers. *Global Biogeochem. Cy.* **2000,** *14*, (1), 373-387.
(38) Liss, P. S.; Merlivat, L., Air-sea exchange rates: Introduction and synthesis. In *The role of Air-Sea Exchange in Geochemical Cycling*, Buat-Menard, P., Ed. D Reidel Publishing Compant: Dodrecht, 1986; pp 113-127.
(39) Andersson, M. E.; Gardfeldt, K.; Wangberg, I.; Stromberg, D., Determination of Henry's law constant for elemental mercury. *Chemosphere* **2008,** *73*, (4), 587-592.
(40) Poissant, L.; Amyot, M.; Pilote, M.; Lean, D., Mercury water-air exchange over the upper St. Lawrence River and Lake Ontario. *Environ. Sci. Technol.* **2000,** *2000*, (34), 3069-3078.
(41) Wilke, C. R.; Chang, P., Correlation of diffusion coefficients in dilute solutions. *Aiche J.* **1955,** *1*, (2), 264-270.
(42) Loux, N. T., A critical assessment of elemental mercury air/water exchange parameters. *Chem. Speciation Bioavail.* **2004,** *16*, (4), 127-138.
(43) Hayduk, W.; Laudie, H., Prediction of diffusion-coefficients for nonelectrolytes in dilute aqueous solutions. *Aiche J.* **1974,** *20*, (3), 611-615.